NASA/TM—2007-214967 AIAA–2007–2293

Design and Optimization of Composite Gyroscope Momentum Wheel Rings

Brett A. Bednarcyk
Ohio Aerospace Institute, Cleveland, Ohio

Steven M. Arnold
Glenn Research Center, Cleveland, Ohio

September 2007

NASA STI Program . . . in Profile

Since its founding, NASA has been dedicated to the advancement of aeronautics and space science. The NASA Scientific and Technical Information (STI) program plays a key part in helping NASA maintain this important role.

The NASA STI Program operates under the auspices of the Agency Chief Information Officer. It collects, organizes, provides for archiving, and disseminates NASA's STI. The NASA STI program provides access to the NASA Aeronautics and Space Database and its public interface, the NASA Technical Reports Server, thus providing one of the largest collections of aeronautical and space science STI in the world. Results are published in both non-NASA channels and by NASA in the NASA STI Report Series, which includes the following report types:

- TECHNICAL PUBLICATION. Reports of completed research or a major significant phase of research that present the results of NASA programs and include extensive data or theoretical analysis. Includes compilations of significant scientific and technical data and information deemed to be of continuing reference value. NASA counterpart of peer-reviewed formal professional papers but has less stringent limitations on manuscript length and extent of graphic presentations.

- TECHNICAL MEMORANDUM. Scientific and technical findings that are preliminary or of specialized interest, e.g., quick release reports, working papers, and bibliographies that contain minimal annotation. Does not contain extensive analysis.

- CONTRACTOR REPORT. Scientific and technical findings by NASA-sponsored contractors and grantees.

- CONFERENCE PUBLICATION. Collected papers from scientific and technical conferences, symposia, seminars, or other meetings sponsored or cosponsored by NASA.

- SPECIAL PUBLICATION. Scientific, technical, or historical information from NASA programs, projects, and missions, often concerned with subjects having substantial public interest.

- TECHNICAL TRANSLATION. English-language translations of foreign scientific and technical material pertinent to NASA's mission.

Specialized services also include creating custom thesauri, building customized databases, organizing and publishing research results.

For more information about the NASA STI program, see the following:

- Access the NASA STI program home page at *http://www.sti.nasa.gov*

- E-mail your question via the Internet to *help@sti.nasa.gov*

- Fax your question to the NASA STI Help Desk at 301–621–0134

- Telephone the NASA STI Help Desk at 301–621–0390

- Write to:
  NASA Center for AeroSpace Information (CASI)
  7115 Standard Drive
  Hanover, MD 21076–1320

NASA/TM—2007-214967 AIAA–2007–2293

Design and Optimization of Composite Gyroscope Momentum Wheel Rings

Brett A. Bednarcyk
Ohio Aerospace Institute, Cleveland, Ohio

Steven M. Arnold
Glenn Research Center, Cleveland, Ohio

Prepared for the
48th Structures, Structural Dynamics, and Materials (SDM) Conference
cosponsored by the AIAA, ASME, ASCE, AHS, and ASC
Honolulu, Hawaii, April 23–26, 2007

National Aeronautics and
Space Administration

Glenn Research Center
Cleveland, Ohio 44135

September 2007

Acknowledgments

The authors gratefully acknowledge the support of Steve Koss at the Naval Research Laboratory.

Level of Review: This material has been technically reviewed by technical management.

Available from

NASA Center for Aerospace Information
7115 Standard Drive
Hanover, MD 21076–1320

National Technical Information Service
5285 Port Royal Road
Springfield, VA 22161

Available electronically at http://gltrs.grc.nasa.gov

Design and Optimization of Composite Gyroscope Momentum Wheel Rings

Brett A. Bednarcyk
Ohio Aerospace Institute
Brook Park, Ohio 44142

Steven M. Arnold
National Aeronautics and Space Administration
Glenn Research Center
Cleveland, Ohio 44135

Abstract

Stress analysis and preliminary design/optimization procedures are presented for gyroscope momentum wheel rings composed of metallic, metal matrix composite, and polymer matrix composite materials. The design of these components involves simultaneously minimizing both true part volume and mass, while maximizing angular momentum. The stress analysis results are combined with an anisotropic failure criterion to formulate a new sizing procedure that provides considerable insight into the design of gyroscope momentum wheel ring components. Results compare the performance of two optimized metallic designs, an optimized SiC/Ti composite design, and an optimized graphite/epoxy composite design. The graphite/epoxy design appears to be far superior to the competitors considered unless a much greater premium is placed on volume efficiency compared to mass efficiency.

I. Introduction

Gyroscopes use the conservation of angular momentum in order to measure or control orientation. Often referred to as control momentum gyroscopes (CMGs), these systems are used in aircraft, satellites, spacecraft, and ships (refs. 1 and 2) (see fig. 1) when they are cost and mass effective. A key component of a gyroscope is the momentum wheel, also sometimes referred to as the CMG flywheel. It is this spinning component that stores the angular momentum that can be used by the system for control or sensing purposes and thus, along with its hub, drives the design of the gyroscope system. While the non-terrestrial applications for gyroscopes demand an optimized light-weight and low-volume design, the momentum wheel design has not typically been optimized. For example, heritage designs have predominantly used a standard operating rotational speed of 6000 rpm on which legacy bearing designs have been based, despite the fact that higher speeds will provide significantly improved mass and volume efficiency (ref. 1). Designs are also often based on one material chosen a priori and a finite element stress analysis to determine the minimum margin under operating conditions (refs. 1 and 3). Clearly, this approach tends to be overly conservative, and a good deal of efficiency that could be captured through design and material selection is being left on the table. Further, with the development of efficient and reliable gyroscopes, additional system weight saving are possible by utilizing the gyroscope for energy storage as well as control (refs. 4 and 5).

This paper presents an analytical stress analysis, applicable to both composite (anisotropic) and metallic (isotropic) gyroscope momentum wheel rings. The stress analysis is combined with an anisotropic failure criterion to enable the failure (rupture) prediction of the momentum wheel ring due to angular velocity and gimbal maneuver loading. A factor of safety is incorporated, and a sizing (optimization) procedure is presented, which was implemented in a computer code. While the method considers only a single rotating ring (rather than multiple momentum wheel rings, the hub, and the shaft), it is highly efficient and thus well suited for preliminary design and sizing studies in which hundreds or thousands of potential designs may be considered. Full system design, requiring a detailed finite element

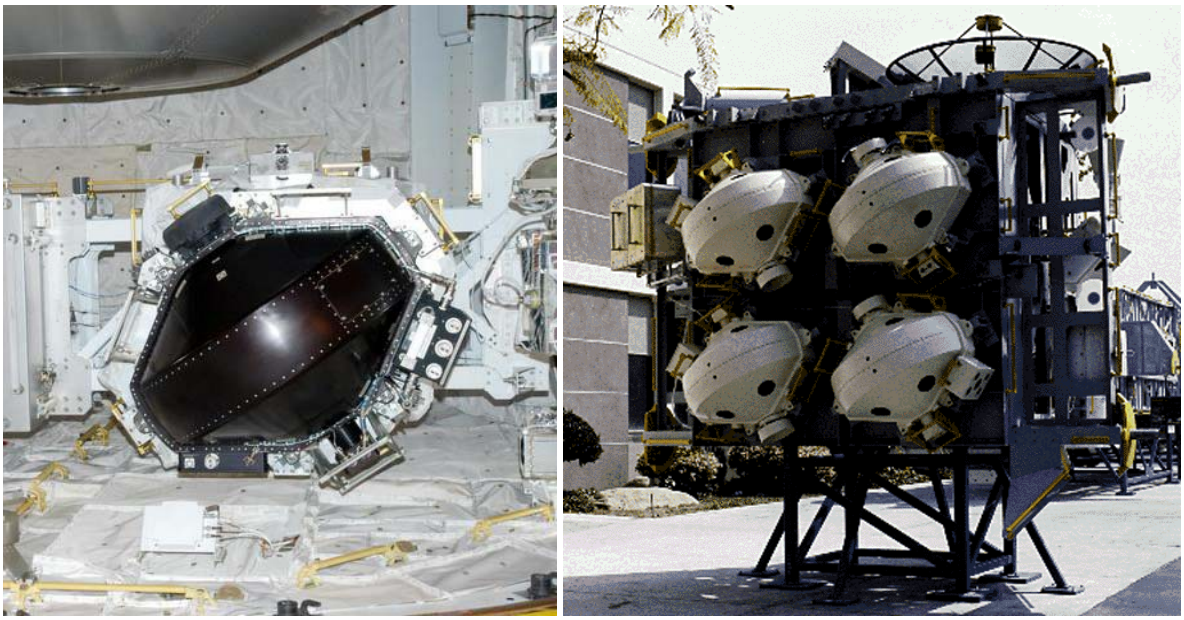

(a) (b)

Figure 1.—Example packaged CMGs from (a) the Space Shuttle Orbiter and (b) the International Space Station (mockup).

stress analysis (cf. ref. 6), would be necessary to implement the designs considered herein into an actual gyroscope design. In the detailed design process, trades between the ring and hub would be considered to arrive at the overall optimum configuration.

Results are presented for two metallic ring designs (stainless steel and AerMet 100) and two composite ring designs (SiC/Ti and graphite/epoxy) with unidirectional circumferential reinforcement. The results illustrate the competing nature of the need to minimize both mass and volume while maximizing angular momentum. A performance index, that combines these competing needs, is developed and applied to the design. Based on this performance index, the graphite/epoxy design emerges as the clear choice among the materials considered when an approximately equal importance is placed on both volume and mass efficiency.

II. Stress Analysis

An annular, circumferentially reinforced, gyroscope rotor momentum wheel ring that is considered is shown in figure 2. As shown, the ring may be subjected to internal and external pressure (possibly associated with press-fitting with additional rings), an angular velocity, ω, and a linear temperature gradient defined by,

$$\Delta T = T_a - T_{ref} + (r-a)\frac{T_b - T_a}{b-a} \tag{1}$$

where a, b, T_a, and T_b, are the inner and outer radii and boundary temperatures (see fig. 2) and T_{ref} is the reference temperature (refs. 7 and 8). We also consider loading due to an out of plane angle change at a rate of $\dot{\theta}$ (e.g., caused by a gimbal maneuver), as shown in figure 3. It is assumed that the out of plane stress caused by this gimbal maneuver is completely decoupled from the momentum wheel ring in plane response. This assumption is valid provided the out of plane stress is much smaller than the in plane stresses, which, as will be shown, is true in the present application. The stress field that results from the problem posed above involves only normal stresses, with in plane components, σ_r and σ_θ, a function of radial position, r, and the decoupled out of plane component, σ_z, a function of distance from the rotor in

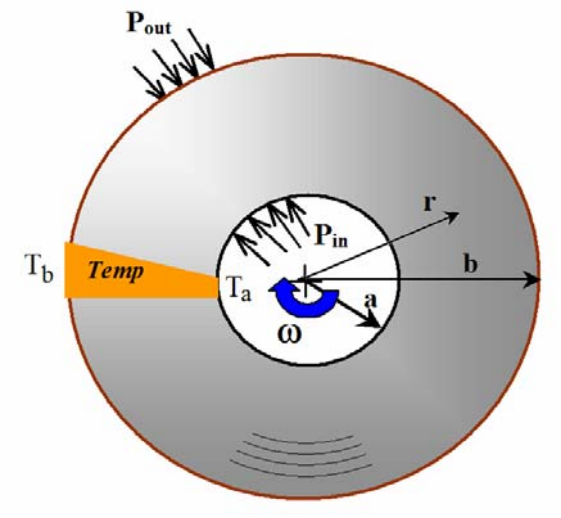

Figure 2.—An annular gyroscope rotor momentum wheel ring with circumferential reinforcement.

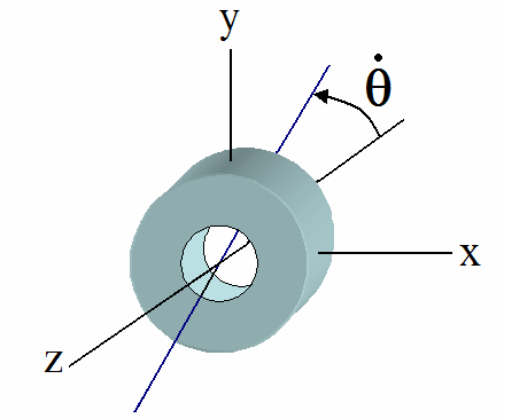

Figure 3.—A gyroscope momentum wheel ring subjected to an out of plane angular change due to a gimbal maneuver.

plane midline (e.g., a function of the coordinate *y* in figure 3). Under these conditions, the equilibrium equations reduce to,

$$\frac{d\sigma_r}{dr} + \frac{\sigma_r - \sigma_\theta}{r} + \rho\omega^2 r = 0 \tag{2}$$

which allows the circumferential stress to be expressed as,

$$\sigma_\theta = \frac{d}{dr}\left(r\sigma_r\right) + \rho\omega^2 r^2 \tag{3}$$

Combining the equilibrium, compatibility, and constitutive equations, along with the assumption that the out of plane stress, σ_z, is small relative to the in plane stresses, the governing equation for the radial stress can be expressed as (see ref. 7 for details),

$$r^2\frac{d^2\sigma_r}{dr^2}+3r\frac{d\sigma_r}{dr}+\left(1-\Sigma^2\right)\sigma_r=Q(r) \tag{4}$$

where $\Sigma=\sqrt{E_L/E_T}$, E_L and E_T are the longitudinal and transverse elastic moduli,

$$\begin{aligned}Q(r)=\frac{1}{b-a}\Big\{&rE_L\left(T_a-T_b\right)\left(2\alpha_L-\alpha_T\right)+a\left[E_L\left(T_b-T_{ref}\right)\left(\alpha_L-\alpha_T\right)+r^2\rho\omega^2\left(3+\nu_L\right)\right]\\&-b\left[E_L\left(T_a-T_{ref}\right)\left(\alpha_L-\alpha_T\right)+r^2\rho\omega^2\left(3+\nu_L\right)\right]\Big\}\end{aligned} \tag{5}$$

α_L and α_T are the longitudinal and transverse coefficients of thermal expansion, ν_L is the longitudinal Poisson ratio, and ρ is the density. The general solution of equation (4) is,

$$\sigma_r=C_1r^{m_1}+C_2r^{m_2}+Q_1(r)-Q_2(r) \tag{6}$$

and from equation (3), the circumferential stress distribution is,

$$\sigma_\theta=C_1\left(m_1+1\right)r^{m_1}+C_2\left(m_2+1\right)r^{m_2}+\left(m_1+1\right)Q_1(r)-\left(m_2+1\right)Q_2(r)+\rho\omega^2r^2 \tag{7}$$

where,

$$Q_1(r)=\frac{r^{m_1}}{m_1-m_2}\int r^{-(m_1+1)}Q(r)\,dr \tag{8}$$

$$Q_2(r)=\frac{r^{m_2}}{m_1-m_2}\int r^{-(m_2+1)}Q(r)\,dr \tag{9}$$

$m_1=-1+\Sigma$, $m_2=-1-\Sigma$, and C_1 and C_2 are constants that can be determined from the boundary conditions.

Limiting attention to the isothermal case with zero internal and external pressure, the normalized in-plane stress fields can be written as,

$$g=\frac{\sigma_r}{\rho\omega^2b^2}=\frac{3+\upsilon_L}{\Sigma^2-9}\left\{\left(\frac{\left(1-X^{3+\Sigma}\right)}{\left(X^{2\Sigma}-1\right)}\left(\frac{r}{b}\right)^{\Sigma-1}\right)-\left(\frac{\left(X^{2\Sigma}-X^{3+\Sigma}\right)}{\left(X^{2\Sigma}-1\right)}\left(\frac{r}{b}\right)^{-1-\Sigma}\right)+\left(\frac{r}{b}\right)^2\right\} \tag{10}$$

$$f=\frac{\sigma_\theta}{\rho\omega^2b^2}=\frac{3+\upsilon_L}{\Sigma^2-9}\left\{\Sigma\frac{\left(1-X^{3+\Sigma}\right)}{\left(X^{2\Sigma}-1\right)}\left(\frac{r}{b}\right)^{\Sigma-1}+\left(\Sigma\frac{\left(X^{2\Sigma}-X^{3+\Sigma}\right)}{\left(X^{2\Sigma}-1\right)}\left(\frac{r}{b}\right)^{-1-\Sigma}\right)+\frac{\left(\Sigma^2+3\upsilon_L\right)}{3+\upsilon_L}\left(\frac{r}{b}\right)^2\right\} \tag{11}$$

where $X=a/b$ and the normalized circumferential and radial stresses, f and g, have been defined. In the case of isotropic materials, equations (10) and (11) reduce to,

$$g=\frac{\sigma_r}{\rho\omega^2b^2}=-\frac{3+\upsilon}{8}\left\{\left(\frac{\left(1-X^4\right)}{\left(X^2-1\right)}\right)-\left(\frac{\left(X^2-X^4\right)}{\left(X^2-1\right)}\left(\frac{r}{b}\right)^{-2}\right)+\left(\frac{r}{b}\right)^2\right\} \tag{12}$$

$$f = \frac{\sigma_\theta}{\rho\omega^2 b^2} = \frac{-(3+\upsilon)}{8}\left\{\frac{\left(1-X^4\right)}{\left(X^2-1\right)} + \left(\frac{\left(X^2-X^4\right)}{\left(X^2-1\right)}\left(\frac{r}{b}\right)^{-2}\right) + \frac{(1+3\upsilon)}{3+\upsilon}\left(\frac{r}{b}\right)^2\right\} \tag{13}$$

The out of plane stress induced by the gimbal maneuver (see fig. 3) is determined from the out of plane moment experienced by the spinning momentum wheel ring due to the out of plane rate of angular change, $\dot{\theta}$. Recall that this out of plane stress is treated as decoupled from the in plane stresses. The out of plane moment is given by

$$M = I_z^G \omega\dot{\theta} \tag{14}$$

where I_z^G is the mass moment of inertia with respect to the *z*-axis (see fig. 3),

$$I_z^G = \frac{\pi}{2}\left(b^4 - a^4\right)\rho t \tag{15}$$

The resulting out of plane stress is given by,

$$\sigma_z = \frac{My}{I_x} \tag{16}$$

where I_x is the area moment of inertia about the *x*-axis,

$$I_x = \frac{\pi}{4}\left(b^4 - a^4\right) \tag{17}$$

and *t* is the out of plane thickness of the momentum wheel ring. Combining equations (14) to (17) yields,

$$h = \frac{\sigma_z}{\rho\omega^2 b^2} = 2\left(\frac{t}{b}\right)\left(\frac{y}{b}\right)\left(\frac{\dot{\theta}}{\omega}\right) \tag{18}$$

In the case where the angular momentum of the momentum wheel ring, $H = I_z^G\omega$, is specified, the out of plane stress can be expressed as,

$$\sigma_z = \frac{4H\dot{\theta}}{\pi b^4\left(1-X^4\right)}y \tag{19}$$

III. Failure Criterion

Because the momentum wheel ring may be circumferentially reinforced, and thus transversely isotropic, a transversely isotropic failure criterion has been adopted that accounts for the multiaxial stress state. This multiaxial criterion is based on an equivalent transversely isotropic effective (J_2-like) stress measure (multiaxial) that is comprised of physically meaningful invariants that represent stress states that are likely to influence strongly the various damage modes within composites (ref. 9). For example: i) the transverse shear stress (I_1) accounts for matrix cracking, ii) the longitudinal shear stress (I_2) dictates interfacial degradation, and iii) the maximum normal stress (I_3) in the fiber direction dictates fiber

breakage. Note that these are not the standard invariants of the stress tensor. All three of the invariants are combined into a function representing the effective transversely isotropic J_2-like invariant,

$$F_{(\,)} = \sqrt{\frac{1}{(\,)_L}\left\{(4\xi_{(\,)}{}^2 - 1)I_1 + \frac{(4\xi_{(\,)}{}^2 - 1)}{\eta_{(\,)}{}^2} I_2 + \frac{9}{4} I_3\right\}} \tag{20}$$

where,

$$\begin{aligned} I_1 &= J_2 - \hat{I} + \frac{1}{4} I_3 & J_2 &= \frac{1}{2} S_{ij} S_{ij} \\ I_2 &= \hat{I} - I_3 & I &= D_{ij} S_{ij} \\ I_3 &= I^2 & \hat{I} &= D_{ij} S_{jk} S_{ki} \\ \xi &= \frac{\sigma_{(\,)_L}}{\sigma_{(\,)_T}} & D_{ij} &= d_i d_j \\ & & S_{ij} &= \sigma_{ij} - \frac{1}{3}\sigma_{kk}\delta_{ij} \end{aligned} \tag{21}$$

and d_i (i = 1, 2, 3) are the components of a unit vector denoting the local fiber direction. Note that within ( ) one can insert either ultimate or yield measures of material failure (or limit load). $\sigma_{(\,)_L}$ and $\sigma_{(\,)_T}$ are thus the longitudinal and transverse limit loads. In case of isotropy F reduces to classical J_2 failure criterion.

IV. Optimization Procedure

Noting that the normalization of the stress components (eqs. (10) to (13) and (18)) eliminates the ω dependence for f and g, but not h, the multiaxial failure criterion, equation (20), can be written in terms of the normalized stress components as,

$$F_{(\,)} = \frac{\rho\omega^2 b^2}{\sigma_{(\,)L}} \sqrt{\xi_{(\,)}^2\left[g^2 - 2gh(\omega) + h(\omega)^2\right] + gh(\omega) - gf - fh(\omega) + f^2} \tag{22}$$

where the ω dependence of h has been indicated. We now assume as before that the out of plane stress (h) is small compared to the in plane stress components, resulting in,

$$F_{(\,)} = \frac{\rho\omega^2 b^2}{\sigma_{(\,)L}} \sqrt{\xi_{(\,)}^2 g^2 - gf + f^2} \tag{23}$$

which can be solved for the maximum allowable angular velocity,

$$\omega_{\max}^2 = \frac{F_{(\,)}^{allowable}\,\sigma_{(\,)L}}{\rho b^2\left[\sqrt{\xi_{(\,)}^2 g^2 - gf + f^2}\right]_{\max}} \tag{24}$$

where the allowable magnitude of the failure criterion function is given by,

$$F_{(\,)}^{allowable} = \frac{0.999}{FS} \tag{25}$$

and FS is the desired factor of safety to be employed in the momentum wheel ring design. A numerator of 0.999 is employed in this expression, rather than 1.0 in order to accommodate a small, but finite value of the out of plane stress. Also in equation (24), the $\left[\ \right]_{\max}$ operator refers to the maximum value of the bracketed term occurring within the momentum wheel ring, which can potentially occur at any radial position.

The momentum wheel ring's angular momentum at the maximum allowable angular velocity is given by,

$$H = I_z^G\, \omega_{\max}(b) = \frac{\pi}{2}\left[1 - X^4\right] b^4 \rho t\, \omega_{\max}(b) \tag{26}$$

where the functional dependence of ω_{max} on the outer diameter, b, has been denoted. Rearranging equation (26) results in,

$$b^4 = \frac{2H}{\pi\left[1 - X^4\right]\rho t\, \omega_{\max}(b)} \tag{27}$$

Equation (27) can be solved by direct iteration for the momentum wheel ring's outer radius, b, which, for a given desired angular momentum (H), rim thickness ratio ($X = a/b$), out of plane thickness (t), and material, will be the minimum outer radius value for the ring that can provide the desired angular momentum. This will also be the lightest and smallest ring that can provide the desired angular momentum.

The momentum wheel ring sizing/optimization procedure can then be summarized as the following steps:

1) For a given H, t, X, $\dot{\theta}$, material, factor of safety, and choice of ultimate or yield limit stress, assume a value (i.e., initial guess) for the momentum wheel ring outer radius, b_0.
2) For iteration i, solve for the stress field throughout the momentum rim (this can be done using a sufficient number of radial solution points) and determine:

$$\left[\sqrt{\xi_{(\,)}^2 g^2 - gf + f^2}\right]_{\max} \tag{28}$$

Note that the radial location corresponding to the maximum value of the bracketed term in equation (28) establishes the controlling failure point in the momentum wheel ring, and this expression is a function of current iteration's value for the outer radius, b_i.

1) Determine the maximum allowable angular velocity associated with b_i,

$$\omega_{\max} = \left\{ \frac{F_{(\,)}^{allowable}\, \sigma_{(\,)L}}{\rho b_i^2 \left[\sqrt{\xi_{(\,)}^2 g^2 - gf + f^2}\right]_{\max}} \right\}^{\frac{1}{2}} \tag{29}$$

2) Determine a new value for the outer radius,

$$b_{i+1} = \left\{ \frac{2H}{\pi\left[1 - X^4\right]\rho t\, \omega_{\max}(b_i)} \right\}^{\frac{1}{4}} \tag{30}$$

3) If b has not converged, set $i = i + 1$ and go to step 2.

4) Perform final check of full failure criterion throughout the momentum wheel ring,

$$F_{(\ )} = \frac{\rho\omega^2 b^2}{\sigma_{(\ )L}} \sqrt{\xi_{(\ )}^2\left[g^2 - 2gh(\omega) + h(\omega)^2\right] + gh(\omega) - gf - fh(\omega) + f^2} \le F_{(\ )}^{allowable} = \frac{0.999}{FS} \tag{31}$$

Violation of this full failure criterion indicates that the out of plane stress may be significant and may call into question the validity of the stress solution. In such a case, the magnitude of the out of plane stress should be examined carefully.

This procedure sizes the ring for a given angular momentum, which is typically the specification to which gyroscope momentum wheel rings are designed and manufactured. The material parameters, out of plane thickness (t), and maximum gimbal rate must also be known. The ratio of inner and outer radii ($X = a/b$) may or may not be known. As such, a computer program was written to size momentum wheel rings based on the above procedure where the value of X is automatically varied from 0.01 to 0.99. Plots of various quantities versus X result and can be used to find the truly optimized momentum wheel ring solution, even across various materials.

V. Results and Discussion

The materials considered for the gyroscope momentum wheel ring in this design study are AerMet 100 (a high-alloy steel), custom 455 stainless steel, a graphite/epoxy composite, and a SiC/Ti metal matrix composite. The material properties for these materials are given in table 1. It is noted that transverse strengths for the composite materials represent static values that have not accounted in anyway for fatigue. Were the ring subjected to a significant number of loading cycles (e.g., spin up and spin down cycles), an appropriate knockdown of these transverse values would be required to account for matrix fatigue cracking. Alternatively, a multi-ring press-fit design, that would preload the ring(s) into compression, could be employed to alleviate the transverse fatigue cracking problem.

TABLE 1.—MATERIAL PROPERTIES. FOR COMPOSITE MATERIALS, DOUBLE VALUES REPRESENT LONGITUDINAL AND TRANSVERSE VALUES, RESPECTIVELY

Material	Volume fraction, (%)	ρ (lbm/in.^{3})	Ultimate strength, (ksi)		Yield strength, (ksi)		Elastic modulus, (Msi)		ν_L
Stainless steel	–	0.284	185		175		29.0		0.26
AerMet 100	–	0.285	294.8		247.4		28.7		0.30
Gr/Ep	60	0.057	302	10	302	10	23.1	1.3	0.282
SiC/Ti	35	0.147	201.6	60.9	201.6	39.6	26.1	17.5	0.272

Throughout this design study, a factor of safety of 2 and a gimbal rate ($\dot{\theta}$) of 1 rad/sec were assumed based on internal communications. Note that a separate study (not shown) indicated that in order for the out of plane stress to reach the magnitude of the material failure stresses, a gimbal rate on the order of 1700 rad/sec would be required. This is clearly unrealistic, and in all cases with the 1 rad/sec gimbal rate, the out of plane stress was small, on the order of 0.1 percent (at most) of the in plane stresses. Also, all results presented have employed the ultimate strength in the design.

We first consider the AerMet 100 material to illustrate how the results can be used to optimize the gyroscope momentum wheel ring design. Figures 4 and 5 show that, as one would expect, higher momentum wheel rings must be larger, and as the rim thickness decreases (higher X values), the outer radius of the ring must be larger to achieve a given momentum.

A better assessment of momentum wheel ring's size is its package volume, defined as,

$$\text{Package Volume} = PkV = \pi b^2 t \tag{32}$$

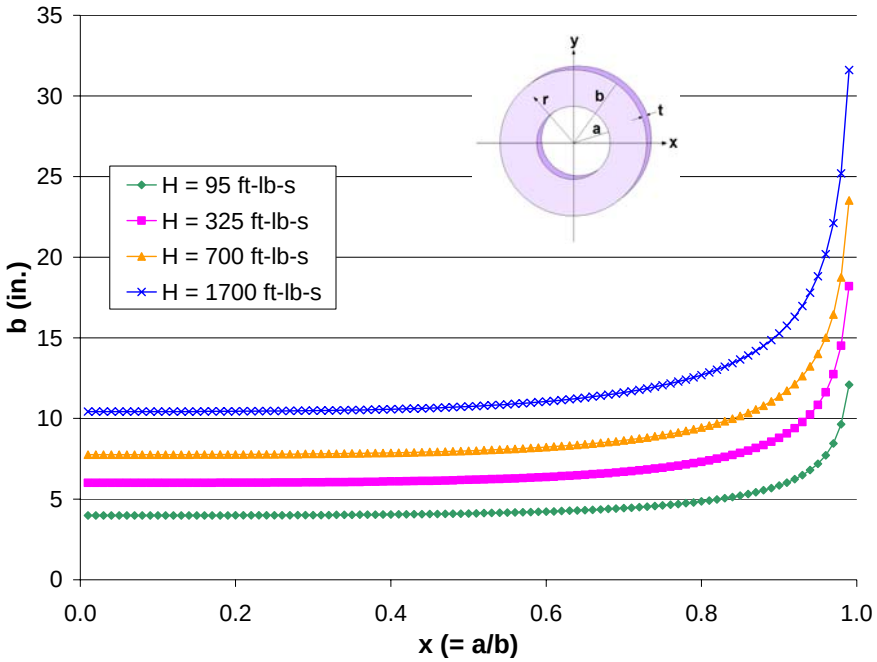

Figure 4.—Optimum outer radius as a function of inner to outer radius ratio (X) for AerMet 100, t = 1 in., and various design-to angular momentum values.

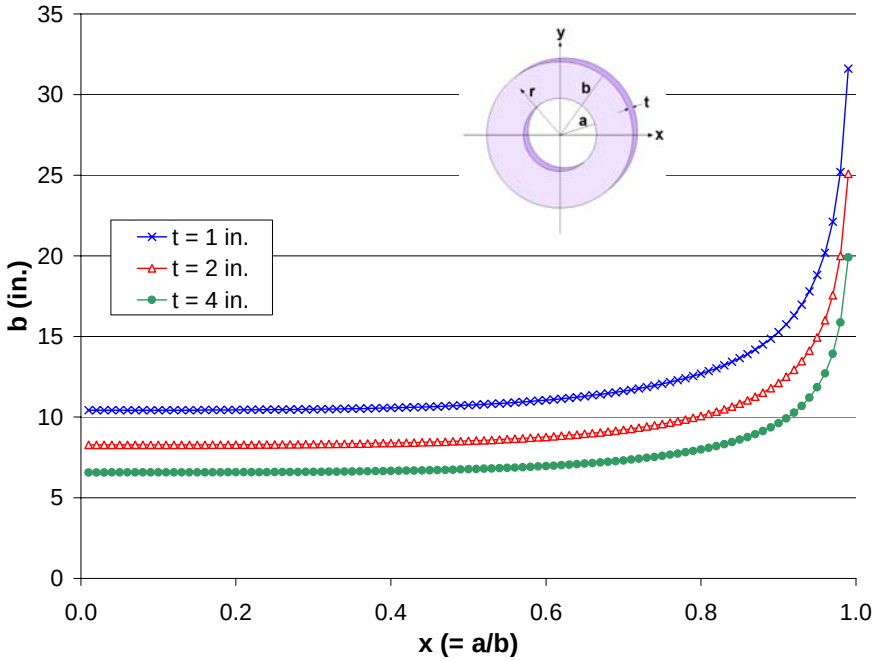

Figure 5.—Optimum outer radius as a function of inner to outer radius ratio (X) for AerMet 100, H = 1700 ft-lb-sec, and various out of plane thicknesses.

This is not the material volume of the momentum wheel ring, but rather the real volume occupied by the ring, where the open internal region contributes to the volume. This is important because it is this volume that must be designed for in housing the gyroscope. Figures 6 and 7 show the package volume of an AerMet 100 momentum wheel ring. The fact that these curves are flat up to approximately $X = 0.60$ indicates that no further volume can be saved by reducing the internal to external radius ratio lower than this value. By the same token, raising this ratio beyond this value brings with it a package volume penalty.

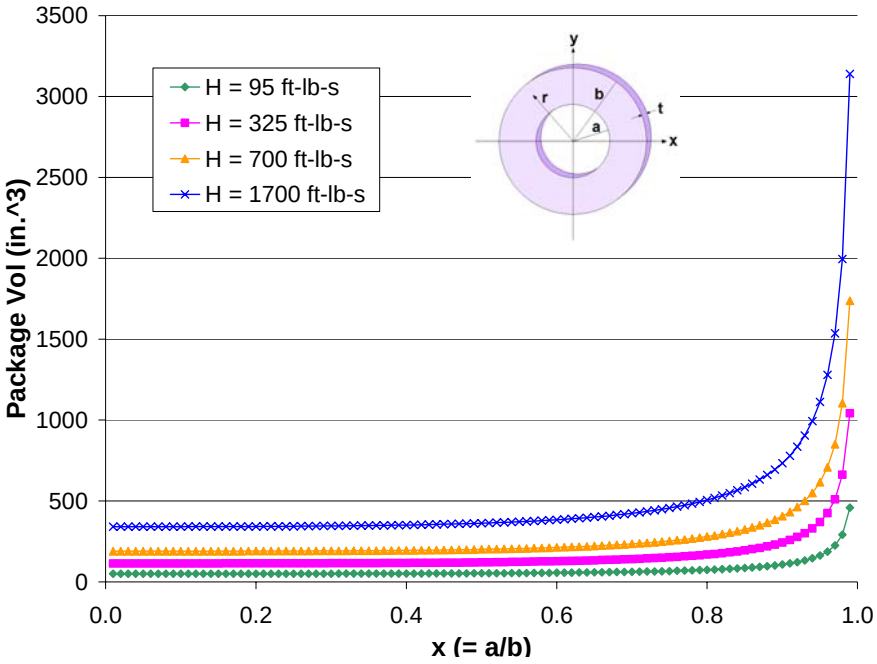

Figure 6.—Optimum package volume as a function of inner to outer radius ratio (X) for AerMet 100, t = 1 in., and various design-to angular momentum values.

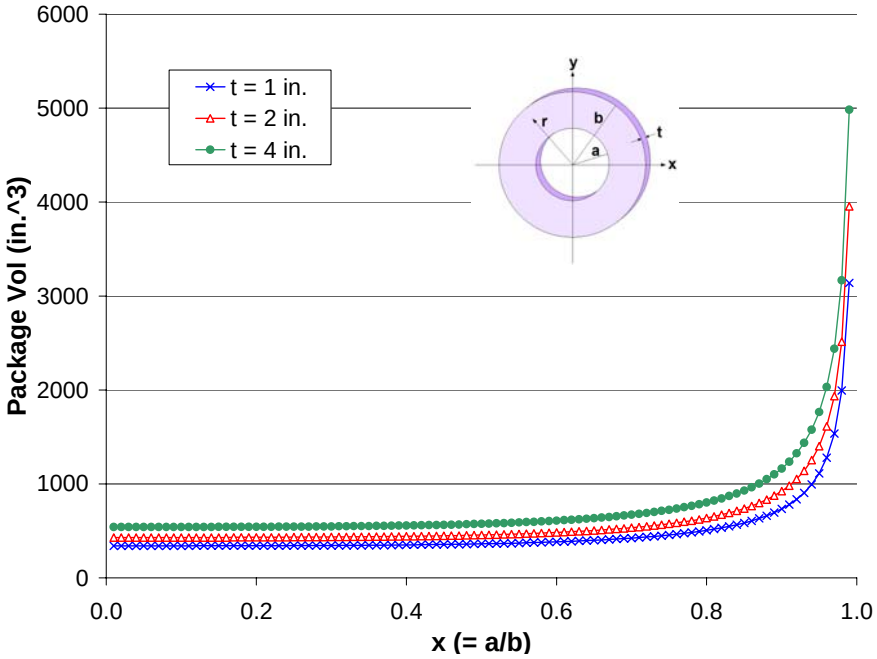

Figure 7.—Optimum package volume as a function of inner to outer radius ratio (X) for AerMet 100, H = 1700 ft-lb-sec, and various out of plane thicknesses.

Figures 8 and 9 show the mass of an AerMet 100 momentum wheel ring. The trend is opposite that of the package volume curves, with higher X values resulting in lower masses. This is because higher X values are associated with lower rim thicknesses and higher outer radii. Large and thin rings provide the best angular momentum per unit mass (as the mass is located further from the center of the ring), but clearly, from figures 6 and 7, a trade off exists between mass and package volume. Both of these factors are important for design as higher mass of the ring is detrimental to the vehicle as is higher package volume due to additional mass required to house a larger gyroscope ring and accompanying system hardware.

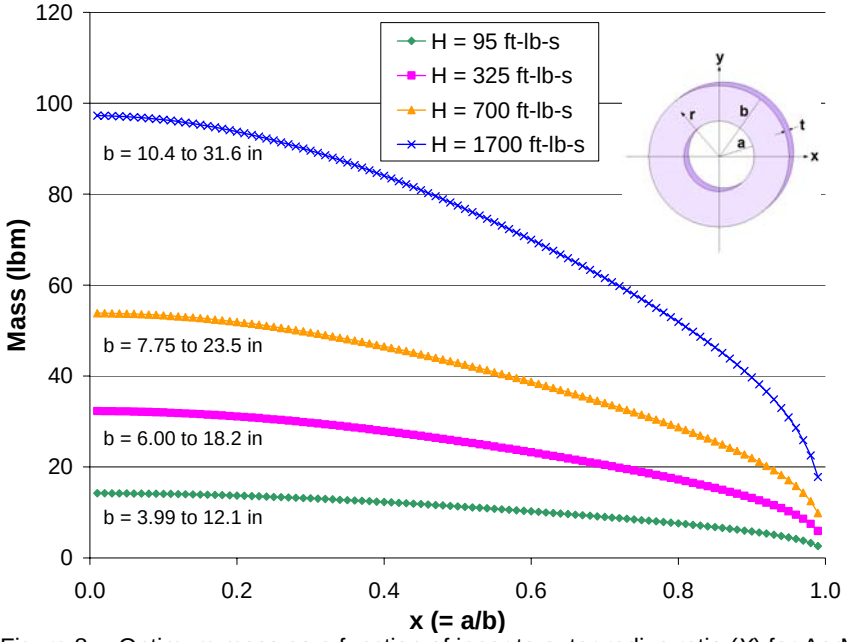

Figure 8.—Optimum mass as a function of inner to outer radius ratio (X) for AerMet 100, t = 1 in., and various design-to angular momentum values. Note that the value of b varies (as indicated) along each curve.

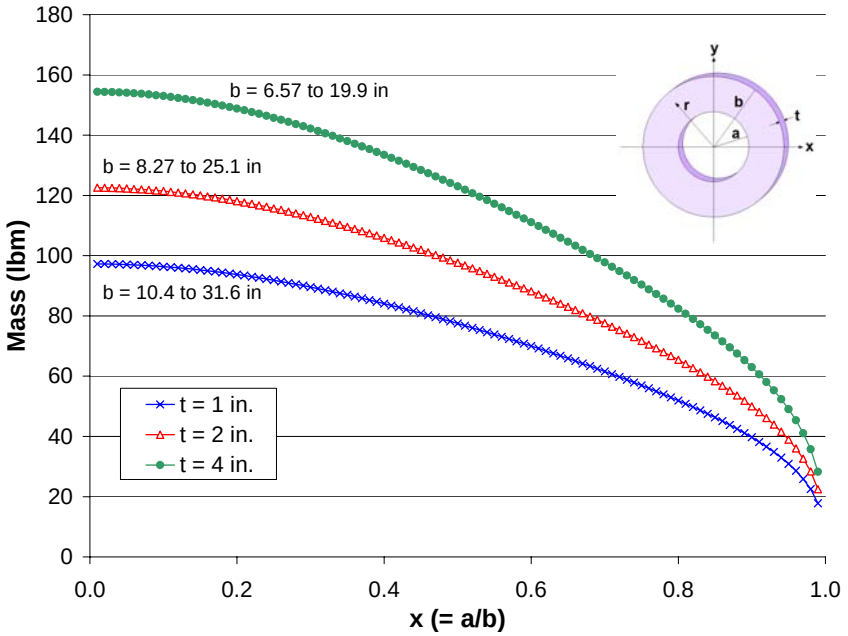

Figure 9.—Optimum mass as a function of inner to outer radius ratio (X) for AerMet 100, H = 1700 ft-lb-sec, and various out of plane thicknesses. Note that the value of b varies (as indicated) along each curve.

In order to quantify and trade the effects of mass and package volume, we consider the angular momentum provided by a ring per unit mass (*H/m*) and per unit package volume (*H/PkV*) as quantities that should simultaneously be maximized. Plots of these two quantities vs. each other are given in figures 10 and 11 for AerMet 100. Because these plots are on a log-log scale, a line of slope 1 corresponds to designs of equal package volume/mass ratios. Such lines also represent equal values of *X*.

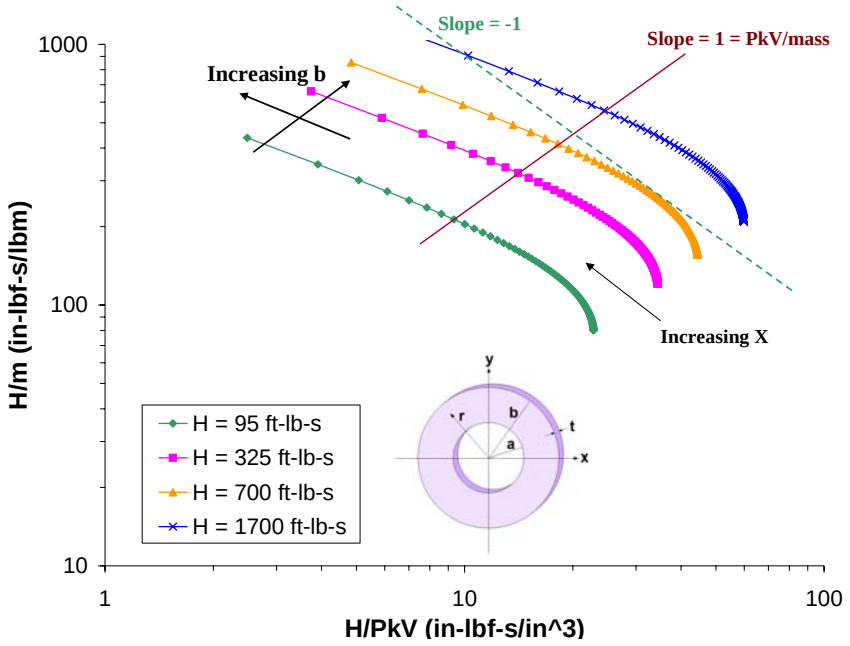

Figure 10.—Angular momentum per unit mass plotted versus angular momentum per unit package volume for AerMet 100, *t* = 1 in., and various design-to angular momentum values. Data points in the upper right hand corner represent the best designs.

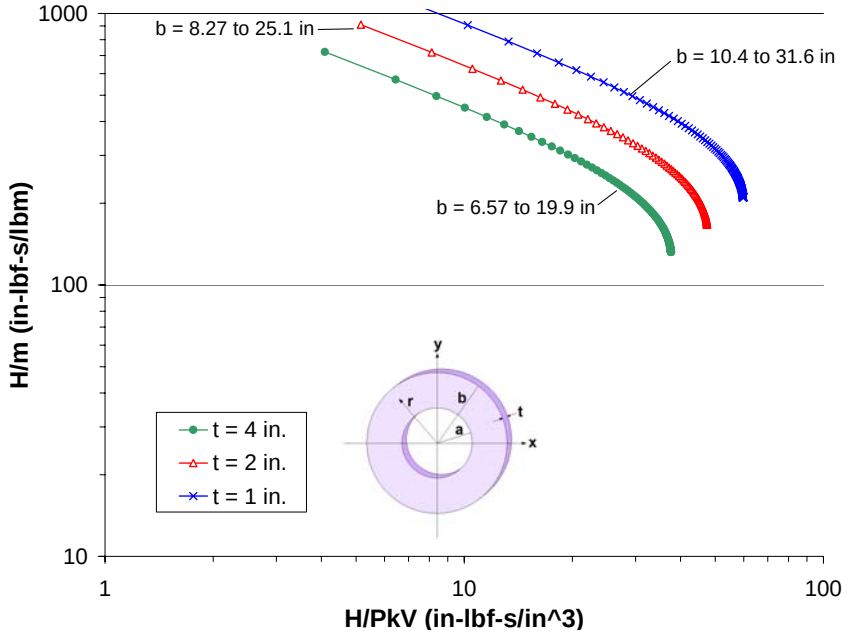

Figure 11.—Angular momentum per unit mass plotted versus angular momentum per unit package volume for AerMet 100, *H* = 1700 ft-lb-sec, and various out of plane thicknesses. Data points in the upper right hand corner represent the best designs.

Lines of slope –1 correspond to equal values of $(H/PkV) \times (H/m)$. Because it is desirable to maximize both of these terms, this concept can be generalized to develop a performance index (PI) for the momentum wheel ring,

$$PI = \left(\frac{H}{PkV}\right)^{\alpha}\left(\frac{H}{m}\right)^{\beta} \tag{33}$$

which, on a log-log plot like those provided in figures 10 and 11, yields lines of slope $-\alpha/\beta$ corresponding to lines of constant PI. The higher and further to the right that the line falls, the better the performance index and the better the design. Therefore, the relative weighting of the importance of package volume and mass minimization with respect to angular momentum can be quantified by the ratio of α to β. For instance, if package volume and mass are given equal importance to the momentum wheel ring design, a slope of –1 results. As shown in figure 10, the shapes of the curves for the different angular momentum values indicate that an optimum design exists that maximizes this performance index.

Figures 12 and 13 now plot this equally weighted performance index, equation (33) with $\alpha = \beta = 1$, versus the inner to outer radius ratio, X. Clearly, in all cases an optimum design can be readily identified as the maximum in the curve. It occurs at $X = 0.74$. This is essentially the point at which the benefits of lower mass associated with higher X values (see figs. 8 and 9) overcome the benefits of lower package volume associated with lower X values (see figs. 6 and 7).

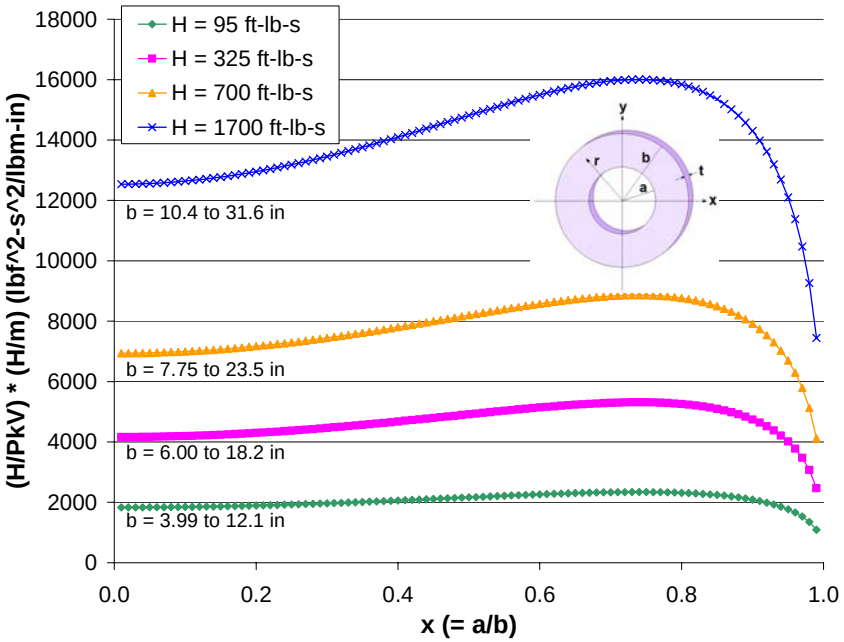

Figure 12.—Equally weighted performance index (see eq. (33)) as a function of inner to outer radius ratio (X) for AerMet 100, t = 1 in., and various values of design-to angular momentum values.

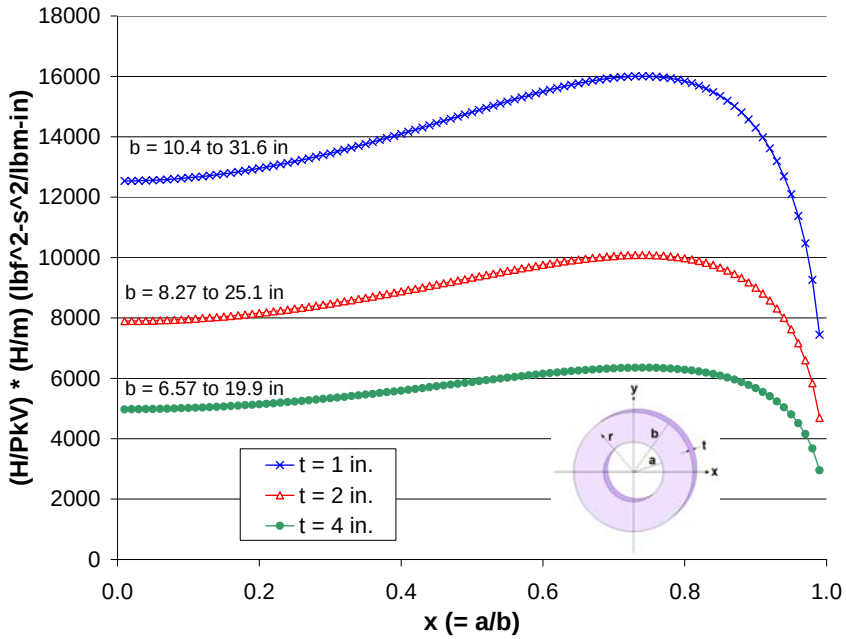

Figure 13.—Equally weighted performance index (see eq. (33)) as a function of inner to outer radius ratio (X) for AerMet 100, H = 1700 ft-lb-sec, and various out of plane thicknesses.

It is now possible to compare the optimum momentum wheel ring designs for the four materials whose properties are given in table 1 (Gr/Ep PMC, SiC/Ti MMC, AerMet 100, and Stainless Steel). Figure 14 shows a plot of the equally weighted performance index versus inner to outer radius ratio (X) in the case of an H = 1700 ft-lbf-sec momentum wheel ring with an out of plane thickness of 1 in. Recall that a factor of safety of 2 has been employed, and the momentum wheel rings have been sized to ultimate. This figure shows that the stainless steel design is inferior over the entire range of X values. At lower X values (below 0.4), the remaining three materials are comparable in terms of performance index. As the value of X increases, the PMC material's performance index increases much more rapidly than those of the other materials and reaches a maximum value that is approximately 75 percent higher than that of the MMC and AerMet 100. This is due to the extreme low density of the PMC. Also, the PMC reaches its optimum design at X = 0.81, while the other three materials reach their optimum designs at X = 0.74. The optimum PMC design corresponds to an outer radius of 16.7 in. and has a maximum tip speed of 844 m/s.

Figure 15 provides a log-log plot of H per unit package volume vs. H per unit mass for all four materials and all four angular velocities considered previously and an out of plane thickness of 1 in. Utilizing a line of slope –1, which corresponds to the equally weighted performance index, it is clear from this figure (as was shown in figure 14) that the PMC material provides the best design (as measured by this performance index). Also plotted is a line of slope –2.7 that intersects an extreme point of both the PMC and AerMet 100 curves. This indicates that in order for the AerMet 100 material design to be competitive with the PMC material design, the importance of package volume must be 2.7 times the importance of mass to the design of the gyroscope momentum wheel ring (see eq. (33)).

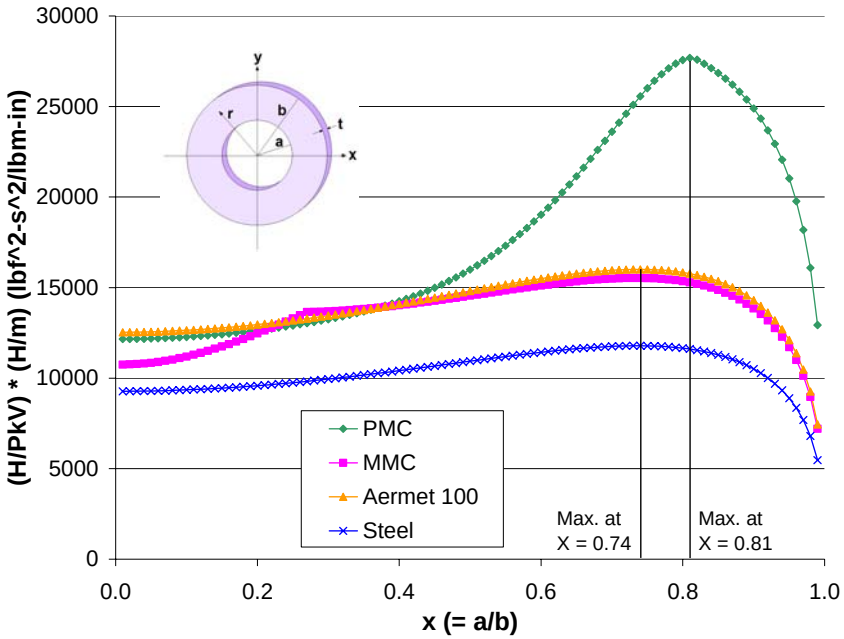

Figure 14.—Comparison of the equally weighted performance index (see eq. (33)) as a function of inner to outer radius ratio (*X*) for the Gr/Ep PMC, SiC/Ti MMC, AerMet 100, and Stainless Steel, *t* = 1 in., and *H* = 1700 ft-lbf-sec.

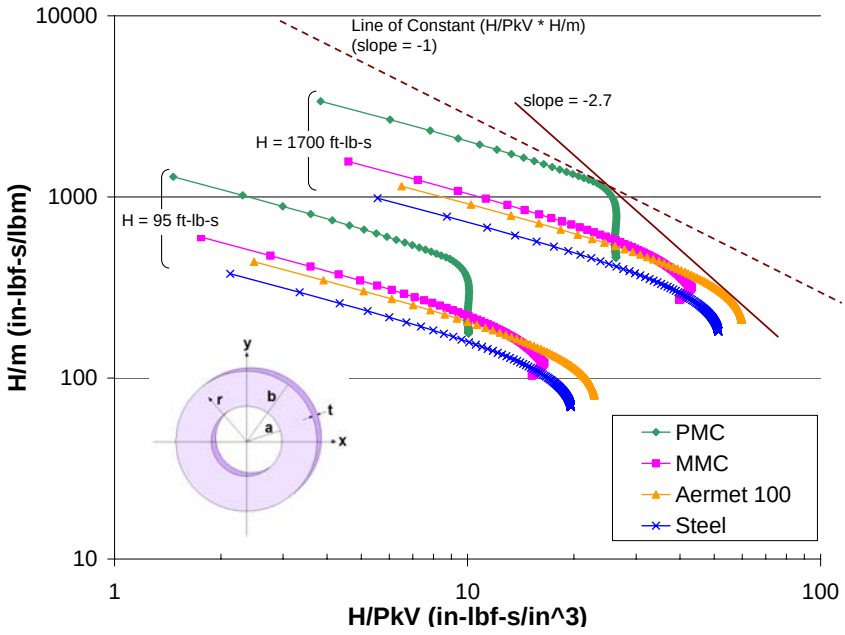

Figure 15.—Comparison of angular momentum per unit mass plotted versus angular momentum per unit package volume for the Gr/Ep PMC, SiC/Ti MMC, AerMet 100, and Stainless Steel, *t* = 1 in, and various values of *H*.

VI. Conclusion

A stress analysis and preliminary sizing/optimization procedure for monolithic and composite gyroscope momentum wheel rings has been developed. This enables improved design efficiency for these critical components that are found in many aerospace and terrestrial applications, and that have typically not been fully optimized in the past. The developed methods and results indicate the presence of a competition between the need to minimize mass and minimize volume, while maximizing angular momentum in both cases. A performance index was developed that combines and quantifies these competing design drivers, given the relative weighting of their importance. Results for two metallic (stainless steel and AerMet 100) and two composite (SiC/Ti and graphite/epoxy) designs indicated that, based on equal weighting of the volume and mass design drivers, the graphite/epoxy momentum wheel ring represents the most efficient design. This is mainly due to the high specific strength of the material compared to the other materials considered. If a much greater importance is placed on volume efficiency compared to mass efficiency, the AerMet 100 design becomes competitive, but only if the relative weighting factor for volume is greater than 2.7 times that for mass.

References

1. Davis, P., "Momentum System Concepts and Trades for the New Class of Smaller Lower Cost Satellites," *Proc. 29th American Astronautical Society Guidance and Control Conference*, AAS 06-23, Breckenridge, CO, Feb. 2006.
2. Fossen, T.I., "Recent Developments in Ship Control Systems Design," *World Superyacht Review*, Sterling Publications Limited, London, 1999.
3. Monaco, A., "Stress Analysis of the ISSA/CMG Flywheel," International Space Station Alpha Hazard Report, Control Moment Gyro (CMG) Rupture, NASA Document 5461508-MT, 1995.
4. McLallin, K.L., Jansen, R.H., Fausz, J., and Bauer, R.D., "Aerospace Flywheel Technology Development for IPACS Applications," NASA/TM–2001-211093, 2001.
5. Kenny, B.H., Jansen, R., Kaczak, P., Densver, T., and Santiago, W., "Demonstration of Single Axis Combined Attitude Control and Energy Storage Using Two Flywheels," NASA/TM–2001-212935, 2004.
6. Gowayed, Y., Abel-Hady, F., Flowers, G.T., and Trudell, J.J., "Optimal Design of Multi-Directional Composite Flywheel Rotors," *Polymer Composites*, vol. 23, pp. 433–441, 2002.
7. Arnold, S. M, Saleeb, A.F., and Al-Zoubi, N.R., "Deformation and Life Analysis of Composite Flywheel Disk and Multi-Disk Systems," NASA/TM–2001-210578, 2001.
8. Arnold, S. M, Saleeb, A.F., and Al-Zoubi, N.R., "Deformation and Life Analysis of Composite Flywheel Disk Systems," *Composites: Part B*, vol. 33, pp. 433–459, 2002.
9. Arnold, S.M. and Kruch, S., "A Differential CDM Model for Fatigue of Unidirectional Metal Matrix Composites," *International Journal of Damage Mechanics*, vol. 3, pp. 170–191, 1994.

REPORT DOCUMENTATION PAGE	Form Approved OMB No. 0704-0188

1. REPORT DATE *(DD-MM-YYYY)*	2. REPORT TYPE	3. DATES COVERED *(From - To)*
01-09-2007	Technical Memorandum	

4. TITLE AND SUBTITLE
Design and Optimization of Composite Gyroscope Momentum Wheel Rings

5a. CONTRACT NUMBER

5b. GRANT NUMBER

5c. PROGRAM ELEMENT NUMBER

6. AUTHOR(S)
Bednarcyk, Brett, A.; Arnold, Steven, M.

5d. PROJECT NUMBER

5e. TASK NUMBER

5f. WORK UNIT NUMBER
WBS 861726.01.03.0555.01

7. PERFORMING ORGANIZATION NAME(S) AND ADDRESS(ES)
National Aeronautics and Space Administration
John H. Glenn Research Center at Lewis Field
Cleveland, Ohio 44135-3191

8. PERFORMING ORGANIZATION REPORT NUMBER
E-16120

9. SPONSORING/MONITORING AGENCY NAME(S) AND ADDRESS(ES)
National Aeronautics and Space Administration
Washington, DC 20546-0001

10. SPONSORING/MONITORS ACRONYM(S)
NASA; AIAA

11. SPONSORING/MONITORING REPORT NUMBER
NASA/TM-2007-214967; AIAA-2007-2293

12. DISTRIBUTION/AVAILABILITY STATEMENT
Unclassified-Unlimited
Subject Categories: 24 and 39
Available electronically at http://gltrs.grc.nasa.gov
This publication is available from the NASA Center for AeroSpace Information, 301-621-0390

13. SUPPLEMENTARY NOTES

14. ABSTRACT
Stress analysis and preliminary design/optimization procedures are presented for gyroscope momentum wheel rings composed of metallic, metal matrix composite, and polymer matrix composite materials. The design of these components involves simultaneously minimizing both true part volume and mass, while maximizing angular momentum. The stress analysis results are combined with an anisotropic failure criterion to formulate a new sizing procedure that provides considerable insight into the design of gyroscope momentum wheel ring components. Results compare the performance of two optimized metallic designs, an optimized SiC/Ti composite design, and an optimized graphite/epoxy composite design. The graphite/epoxy design appears to be far superior to the competitors considered unless a much greater premium is placed on volume efficiency compared to mass efficiency.

15. SUBJECT TERMS
Gyroscope; Angular momentum; Failure; Stress analysis; Flywheels; Graphite-epoxy composites; Stainless steels; Design analysis; Angular velocity; Metal matrix composites; Computer programs; Composite materials; Design optimization; Failure analysis

16. SECURITY CLASSIFICATION OF:			17. LIMITATION OF ABSTRACT	18. NUMBER OF PAGES	19a. NAME OF RESPONSIBLE PERSON
a. REPORT	b. ABSTRACT	c. THIS PAGE			STI Help Desk (email:help@sti.nasa.gov)
U	U	U	UU	22	19b. TELEPHONE NUMBER *(include area code)* 301-621-0390